Instrumentation for the accurate measurement of phase and amplitude in optical tomography

Ilkka Nissilä,[a] Kalle Kotilahti, Kim Fallström[b], and Toivo Katila
Laboratory of Biomedical Engineering, Helsinki University of Technology, P. O. Box 2200, 02015 HUT, Finland

(Received 13 December 2001; accepted for publication 2 June 2002)

A single-channel prototype for a frequency-domain optical tomography system is presented. The two main goals in the design of the system were the measurement of phase with minimal systematic errors and a high enough signal-to-noise ratio to detect the small changes in the absorption of brain tissue during brain activity. Although the system inherently is an imaging system, the aspects of the system that relate to multichannel operation will be published separately, as this part of the system is not yet finished. The instrument is described in detail, including the radio-frequency system, the light detection system, and the light source. Factors that affect the accuracy of the measured phase include phase drift, radio-frequency coupling between the source and detector electronics, phase-amplitude cross talk, and others. To increase the range of intensities that can be measured, the gain of the detector is adjusted while keeping the mean anode current small compared with the quiescent current through the voltage bleeder of the photomultiplier tube so that cross talk is avoided. The calibration of the measurements is considered, and the data measured on a phantom are compared with a time-resolved instrument as well as with a finite-element forward model. The instrument allows the measurement of phase to an accuracy of 0.5° between 80 fW and 80 nW at a modulation frequency of 100 MHz, giving a dynamic range of $1{:}10^6$. With a time constant of 0.3 s, phase noise is 0.5° at 1 pW and decreases to 0.06° in a typical activation measurement at 3 cm separation between the optodes. Amplitude noise is 0.8% at 1 pW and 0.1% at 3 cm separation.
 [DOI: 10.1063/1.1497496]

I. INTRODUCTION

Near-infrared spectroscopy (NIRS) has been a subject of intense study in recent years. The absorption of near-infrared light in tissue is strongly dependent on the concentrations of certain molecules, notably oxy- and deoxyhemoglobin, and cytochrome oxidase, which are of physiological interest. NIRS can be used to detect and monitor changes in the concentrations of these molecules in the underlying tissue.[1,2] The absorption of light between the wavelengths 700 and 900 nm is low enough so that light having transmitted through several centimeters of tissue can be detected.

A general model for describing photon transport in tissue is the radiative transfer equation (RTE). Since the RTE is computationally expensive to solve, a number of approximations have been developed for special cases. The diffusion equation, which is applicable in highly scattering domains, is often used as the forward model in optical tomography.[3,4] The optical properties in this model are the absorption and transport scattering coefficients μ_a and μ_s', and the index of refraction n.

Three basic categories of instruments exist. The simplest instruments measure only the intensity of the light.[5–7] Time-domain (TD) instruments measure the distribution of travel times of the photons through tissue [temporal point spread function, (TPSF)].[8–12] Frequency-domain instruments use a high-frequency intensity modulated source and measure the amplitude and phase of the detected light, at one or several modulation frequencies.[13–17]

The measurements may be relative or absolute. If measurements are made before and after a change in the optical properties of the tissue takes place, the differences in the measured data can be used to obtain images that show the location of the changes in optical properties. The advantage of this method is that no absolute calibration of the instrument is required, and the changes may be so small that a linear model can be used for reconstruction. In addition, many technical problems such as instrumental stability and obtaining the precise position of the optodes become less important. The heterogeneity of tissue can be resolved by an absolute measurement together with a nonlinear model for reconstruction. In reality, all instruments measure relative values, and absolute measurements require calibration. The calibration may be performed using a special calibration tool, the geometry and attenuation of which is known separately. In certain cases the calibration can be made on a phantom, the geometry of which is the same as that of the imaged object, if the optical properties have been measured separately.[13,18,19]

Optical imaging using diffuse near-infrared light has several applications. Existing methods for the noninvasive study of brain function include functional magnetic reso-

[a]Author to whom correspondence should be addressed; electronic mail: ilkka.nissila@hut.fi
[b]Laboratory of Physics, Helsinki University of Technology.

nance imaging (fMRI), electroencephalography (EEG), and magnetoencephalography (MEG). Optical imaging is well suited to studies on children,[5,20,21] and it is relatively insensitive to electromagnetic noise. Another application researched by the optical imaging community is the detection of breast cancer.[8,10,13,22,23] Monitoring the neonatal brain with optical tomography could provide early warning of circulatory problems. It is also possible to monitor and image muscle activity.

The instrument being developed at Helsinki University of Technology is based on the frequency-domain principle. The instrument is able to measure amplitude and phase accurately ($<0.5°$) with a high signal-to-noise ratio (SNR) over a wide dynamic range of intensities ($>1:10^6$), thus making it suitable for both brain activation imaging and optical tomography. In this article, we describe the implementation of the system and the principle of calibration. The radio-frequency signal sources are synchronized with the sampling frequency of the digital lock-in amplifier, and the radio-frequency interference between the transmitting and receiving electronics has been minimized to increase the dynamic range. To avoid phase-amplitude cross talk, the measurements are performed at low values of the anode current to avoid disturbing the balance of the voltage bleeder circuit. The H6780-20 photomultiplier tube (PMT) is used as the detector due to its high NIR sensitivity, fast response time, and relatively small phase-amplitude cross talk. The low hysteresis of the H6780-20 makes rapid source multiplexing and PMT gain switching practical, leading to a relatively inexpensive and precise multichannel implementation.

II. IMPLEMENTATION

A. Radio-frequency system

The instrument is based on the heterodyne principle, and the bandwidth of the high-frequency electrical components is from 100 to 500 MHz. The purpose of the wideband implementation is to study the effect of the modulation frequency on phase noise and the dynamic range.

The transmitted light is modulated at a radio frequency (rf) generated by a signal generator (HP 8648A), although a simple fixed-frequency oscillator could be used as well to reduce cost. To detect phase and amplitude with a digital lock-in amplifier (LIA), the rf signal is converted to an intermediate cross-correlation frequency (10–50 kHz) using a mixer and a second rf signal source. The second rf source has a voltage-controlled frequency, so that the cross-correlation frequency can be precisely synchronized to the sampling frequency of the lock-in amplifier. This reduces phase noise and drift.

A commercial digital lock-in amplifier (Stanford Research, Inc., SR810) was used in testing the instrument. The LIA generates a square wave, which is tracked by the type II phase detector [(PD), Philips 74HCT4046A] in the phase-locked loop (PLL). The PD takes the LIA-generated square wave and the mixer-produced intermediate frequency (IF) signal as inputs, and outputs a three-state signal, which depends on the order of raising edges of the two transistor-transistor logic (TTL) input signals. This signal is low-pass

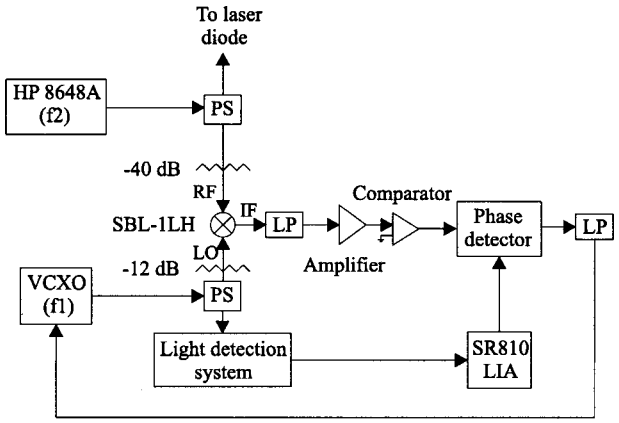

FIG. 1. Radio-frequency system including the signal sources synchronized using a phase-locked loop.

filtered by the loop filter. The dc component is proportional to the phase difference between the two signals. The output of the loop filter controls the frequency of the VCXO (Miteq XT-01-100.01-C-T-15P for 100 MHz and XTM-450.02-C-T-15P for 450 MHz) directly. In addition to the dc component, there is ripple at twice the IF frequency. Since the phase detector output is proportional to V_{CC}, a low-noise regulator circuit is needed to avoid increased phase noise (Fig. 1).

The rf signal from the detector is amplified by 40 dB and mixed with the LO drive to obtain the signal that is measured by the LIA. The receiving mixer (Mini-Circuits TUF-5H) has a wide dynamic range (up to +14 dBm rf) to avoid phase-amplitude cross talk caused by saturation. The relatively large LO drive may be a source of heat-induced drift. Attenuators have been placed between the splitters and the mixers to reduce transmitter–receiver coupling (Fig. 2).

B. Light detection

The detector we currently use is the Hamamatsu H6780-20 photosensormodule, which consists of the R7400U-20 photomultiplier tube and a high-voltage supply. The detector has a short rise time (0.76 ns) and a wide dynamic range (the anode current can be from 2 nA to 100 μA). For a PMT, it is relatively insensitive to external magnetic fields. It is based on a multialkali photocathode, and due to increased cathode thickness over previous models, its sensitivity is very high up to 830 nm, after which it drops rapidly. The R7400U series PMTs have very small hysteresis,[24] which is very important in optical tomography,

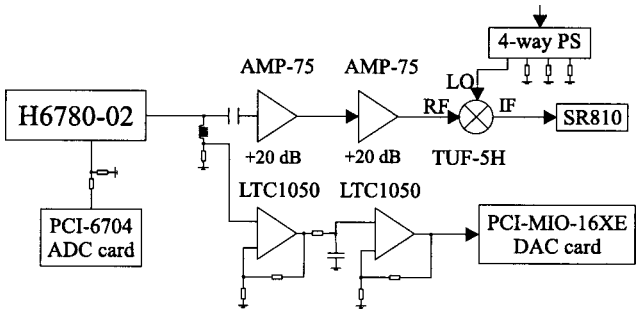

FIG. 2. The PMT with rf and dc amplifier circuits.

since switching the active light source position causes rapid changes in the intensity of detected light as well as the high voltage in our implementation.

Being physically small, the R7400U-20 PMT has a short electron transit time spread [FWHM = 230 ps at 800 V (Ref. 24)]. Thus, it is relatively rare that two pulses partially overlap each other if the anode current is not very high. When several pulses do overlap, the voltage distribution in the bleeder is momentarily disturbed. The changes in the high voltages between the dynodes change the motion of the electrons, changing the signal transmission time and gain. This is a source of phase-amplitude cross talk.

Optical fibers are used to deliver the light on the surface of the tissue or phantom studied, and fiber bundles to collect the light onto the photocathode. The fiber bundles should be as lightweight and flexible as possible to minimize the torques applied to the system that is used to mount the fibers on the tissue. Fibers with a large numerical aperture (NA) have a wider angle of acceptance and they gather more light from a diffuse source than fibers with a small NA. The side effect of a large NA is increased temporal dispersion, which makes them more prone to amplitude and phase changes when bent. Currently, we use bundles with an internal diameter of 2.5 mm and numerical aperture of 0.22 made by CeramOptec, Inc.

The accurate measurement of phase and amplitude can be made only if the amplitude of the signal is within a certain range. The upper limit of this range is determined by the point where the anode current is large enough that phase-amplitude cross talk becomes significant. For the H6780-20, this is approximately 0.1 μA. The lower limit is determined by the amplification of the system and the magnitude of the leak signal from the source to the detector side. The rms amplitude of the leak signal as measured by the LIA is approximately 60 nV at 100 MHz (+5 dBm rf), and 0.7 μV at 450 MHz (+8 dBm rf). If a reactive impedance matching circuit is used, the 100 MHz leak signal is only 40 nV, and it can be reduced further by selecting optimal mixers for the frequency.

C. Light source

The light source for the instrument is a single-mode semiconductor laser diode. Special attention was given to the stability of the measurement of phase, and a temperature stabilizer was implemented to reduce changes in the wavelength, amplitude, and phase of the light emitted by the laser diode.

The laser diode is driven by a dc current (typically, 20–100 mA), which is combined with the rf signal using either a resistive or a reactive impedance matching and biasing circuit.

The mount was carefully designed to minimize rf leaks. The thermoelectric elements and the temperature sensor were placed in close proximity of the laser diode. The control circuit in Fig. 3 was used with a discrete-time proportional-integral derivative (PID) control algorithm.[25]

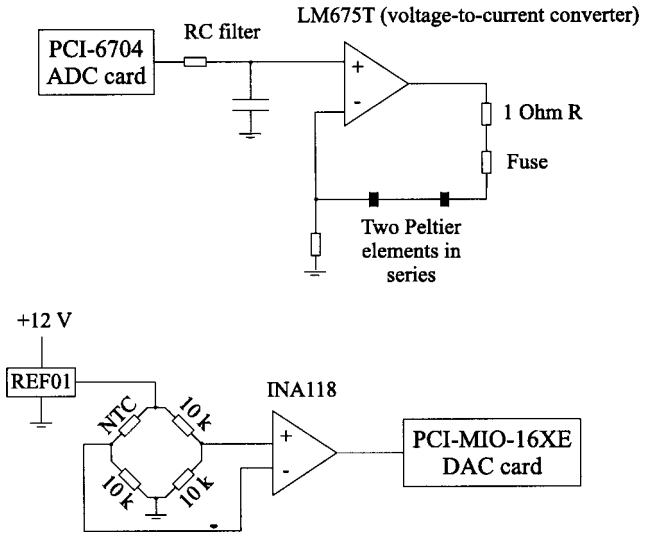

FIG. 3. Temperature stabilizer circuit for the laser diode.

D. rf shielding

The circuits in the rf system have been shielded within boxes milled from aluminum. The coaxial cable used for most signals is RG-223/U, the one exception being the signal from the detector box to the receiving mixer box, which is carried by an RG-400/U cable. The PMT preamplifiers are included within the case containing the PMT module itself. Ferrites have been used around both ends of each coaxial cable, as well as the cables delivering dc power to the active circuits.

III. CALIBRATION

In order to use the data obtained with the instrument for the imaging of the true optical properties, the frequency response of the instrument needs to be measured. In this article, we concentrate on the single-frequency case (100 MHz).

The amplitude and phase can be calibrated with a tissue-like solid calibration phantom, if the optical properties are known and a model describing the propagation of photons in the medium is available. The coupling factors between the optical fibers and the phantom become a part of the calibration.

A more direct approach to calibration can be used for phase. A calibration tool, which holds the source fiber and the detector fiber bundle facing each other at a short distance, was made. A diffusing paper was placed in front of the detector fiber bundle, and two gelatin neutral density filters (4 OD) were placed between the source fiber and the diffuser. The idea for the absolute calibration tool has been presented in (Ref. 18). The accuracy of the calibration depends on how isotropic the light is after going through the paper, which should be single scattering. To avoid the effects of severe drift, a warm-up time of 15–30 min is recommended before the absolute calibration.

The performance of the instrument was measured without a separate reference channel. A reference channel would reduce the system drift caused by the light source and the parts of the rf electronics shared by the detection channels,

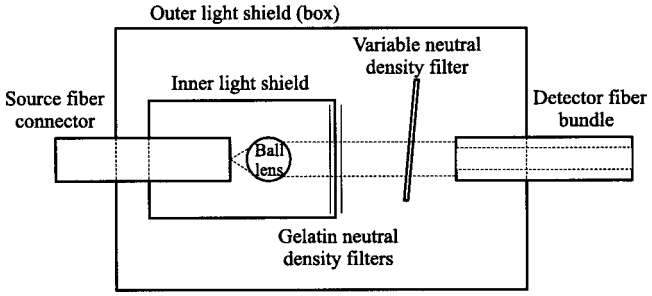

FIG. 4. Optical setup for the measurement of phase-amplitude cross talk.

provided that the same detector type is used for all channels. The absolute calibration tool could be a permanent part of the reference channel. However, subtracting the reference signal from the measurements may increase noise and the procedure does not correct for interchannel drift.

An optical setup was constructed for the measurement of phase-amplitude cross talk (Fig. 4). The light from the source fiber is collimated using a ball lens, and the collimated light is attenuated by a choice of absorbing gelatin neutral density filters. A variable neutral density filter can be rotated to adjust the light incident on the detecting fiber bundle. The collimated beam should be wide enough to cover the active area of the bundle, so that slight changes in the angle of the filter wheel do not significantly affect the measurement, even if the individual fibers of the bundle have slightly different lengths.

The intensity of the light can be adjusted over a 4 OD range by rotating the filter wheel. The dependency of the phase on the amplitude was measured for each of the high-voltage values used in the measurements; i.e., from 300 to 900 V in 100 V steps. The intensity was first set to the lowest value, and it was then increased in discrete steps to reduce the effects of hysteresis on the results. The intensity was increased until the mean anode current reached a value of 1 μA, and then it was decreased in steps to the lowest value available. This procedure was performed twice to investigate the reliability of the measurement. For each high-voltage setting, the total measurement time was 10 min. The phase, amplitude, and anode current were averaged within each step to reduce noise.

In summary of the observations made based on the measurements, we note that the PMT is not quite stable at the intensities used for the cross-talk measurements at 300 and 400 V. This could be a result of photocathode heating. Phase-amplitude cross talk depended on the incident intensity and high voltage, and we found that its effect was below 0.2° for $i_a < 0.2$ μA and increased rapidly for $i_a > 0.5$ μA.

If it is necessary to operate the PMT at anode currents higher than 0.1 μA, a look-up table correcting for the dependency of the phase on the mean anode current can be constructed from the cross-talk measurements for each of the high voltages used. This procedure requires a very careful measurement of the cross talk, preferably using a stepper motor to control the variable neutral density filter and very long measurement times. The rf leak can be partially compensated in software if necessary.[26] Neither of these software correction schemes was used in our case.

TABLE I. System performance figures.

Modulation frequency	100 MHz	450 MHz
Amplitude noise (%)	0.1	0.2
Phase noise (°)	0.06	0.07
Amplitude drift (%/h)	0.6	1
Phase drift (°/h)	0.06	1
Noise-equivalent power (fW)	3	200

Adjusting the high voltage (HV) changes both phase and amplitude. The dependencies have been denoted $A_{\mathrm{HV\ effect}}(V)$ and $\varphi_{\mathrm{HV\ effect}}(V)$, where V is the high voltage. The expressions for the calculation of the corrected amplitude and phase are

$$A_{\mathrm{true}} = \frac{A_{\mathrm{meas}}}{A_{\mathrm{HV\ effect}}(V_{\mathrm{meas}})},$$

and

$$\varphi_{\mathrm{true}} = \varphi_{\mathrm{meas}} - \varphi_{\mathrm{HV\ effect}}(V_{\mathrm{meas}}) + \varphi_{\mathrm{HV\ effect}}(V_{\mathrm{abs}}) - \varphi_{\mathrm{ACT\ meas}} + \varphi_{\mathrm{ACT\ true}} - \varphi_{\mathrm{cross\ talk}}(V_{\mathrm{meas}}, i_{\mathrm{anode}}),$$

where A_{true} is the corrected amplitude, A_{meas} is the measured amplitude, V_{meas} is the high-voltage setting during the measurement, φ_{true} is the absolute phase, φ_{meas} is the measured phase, V_{abs} is the high voltage setting used in the absolute calibration, $\varphi_{\mathrm{ACT\ meas}}$ is the phase measured using the absolute calibration tool (normally at 600 V), $\varphi_{\mathrm{ACT\ true}}$ is the true phase of the absolute calibration tool (corresponding to the distance traveled by the photons between the source and detector fibers in the tool), and $\varphi_{\mathrm{cross\ talk}}(V_{\mathrm{meas}}, i_{\mathrm{anode}})$ is the phase-amplitude cross talk, if present.

An estimate of the accuracy of the measurement of phase can be made by adding up the errors in each step of the calibration. The systematic error made using the absolute calibration tool is not known, and the effect of the bending of the optical fibers has not been rigorously tested. The shot noise of the actual measurement is stochastic and is not considered here. The remaining errors contributing to the absolute measurement error are the random errors (mostly due to the finite time used for each calibration step) in the high-voltage calibration, the absolute calibration, the cross-talk measurement, and the drift. These factors add up to $\sqrt{(0.2°)^2+(0.1°)^2+(0.2°)^2+(0.1°)^2} \approx 0.3°$.

IV. PERFORMANCE

The signal and noise were recorded using a phantom with attenuation similar to the human forehead using a distance of 3 cm between the source and the detector fibers. A Roithner RLT80810MG laser diode with a nominal optical power of 10 mW and wavelength of 808 nm was used. The optical power coupled to the source fiber was 3.5 mW, with a modulation depth of 70% at 100 MHz. The time constant in the lock-in amplifier was 0.3 s, with −6 dB/octave roll off. Slow changes in the amplitude and phase (drift) were quantified based on a 2 h measurement in a dark room without people. The system was allowed the normal warm up time of 30 min. Phase and amplitude were measured for 2 h and low-pass filtered at 30 mHz, and the drift was considered to

TABLE II. rf system performance without the optics.

Modulation frequency	100 MHz	450 MHz
Amplitude noise (%)	0.005	0.007
Phase noise (°)	0.004	0.007
Amplitude drift (%/h)	0.05	0.3
Phase drift (°/h)	0.03	0.6

be the difference between the largest and smallest signal value divided by the transition time. The noise-equivalent power (NEP) is the dc intensity incident on the PMT that gives an ac amplitude SNR of 1 (Table I). The noise and drift of the radio-frequency system operated in a closed loop without the light source and the detector are listed in Table II.

The range of intensities for which the errors in phase caused by the radio frequency leak and phase-amplitude cross talk are below 0.5° at 100 MHz is from 80 fW (50 fW for a reactive impedance matching circuit) to 80 nW, giving a dynamic range of 1×10^6.

Figure 5 illustrates the phase noise and the relative amplitude noise as a function of the intensity of the light incident on the detector.

V. PHANTOM STUDY

The instrument was used to record data for a cylindrical phantom[27,28] using the older H6780-02 PMT. The phantom is homogeneous apart from three perturbations, and we measured the phantom in the plane containing an absorbing perturbation. The measurement was performed for a single source position and 15 detector positions, 30 s each (Fig. 6).

The three-dimensional complex forward solver of the TOAST reconstruction software package was used to calculate simulated data for comparison.[29] The isotropic source model and the Robin boundary condition were used. A cylindrical mesh was generated and the absorbing perturbation was modeled approximately and kept constant relative to the background at $\mu_{a,\mathrm{pert}}=10\times\mu_a$ and $\mu'_{s,\mathrm{pert}}=\mu'_s$. The amplitude calibration constant M, and the background optical properties μ_a and μ'_s were varied to minimize the mean-square error between the measured and simulated phase and logarithm of amplitude. The residual mean-square error is 1.7%. The optical properties were found to be $\mu_a=0.0075\ \mathrm{mm}^{-1}$ and $\mu'_s=1.1\ \mathrm{mm}^{-1}$ (Fig. 7).

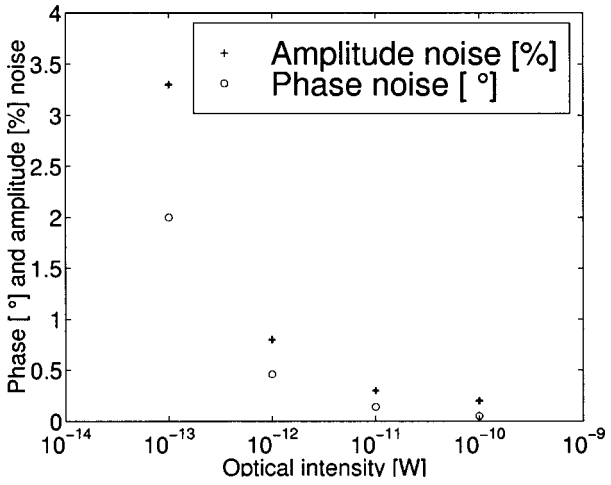

FIG. 5. (a) Phase noise (○) and amplitude noise (+) as a function of the optical power of the incident light. Modulation frequency 100 MHz and time constant 0.3 s.

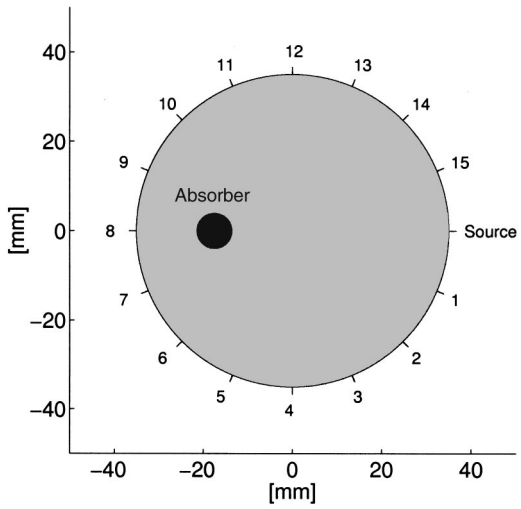

FIG. 6. Structure of the section of the cylindrical phantom that was measured.

Mean time data recorded at 780 nm by the UCL MONSTIR system[12] were also available for comparison. Although phase and mean time are not identical data types, at 100

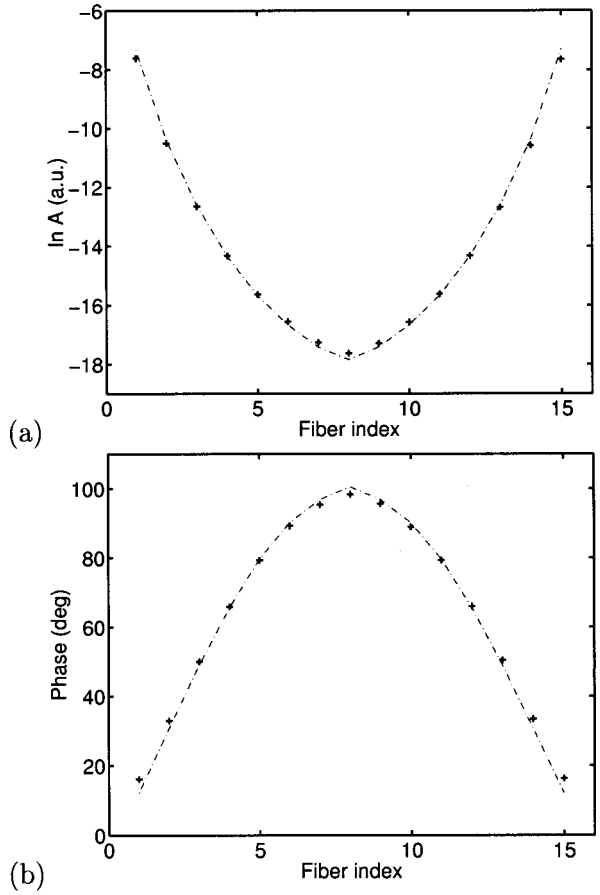

FIG. 7. (a) Amplitude and (b) phase as a function of fiber position. "+" = measured, "-·" = simulated data.

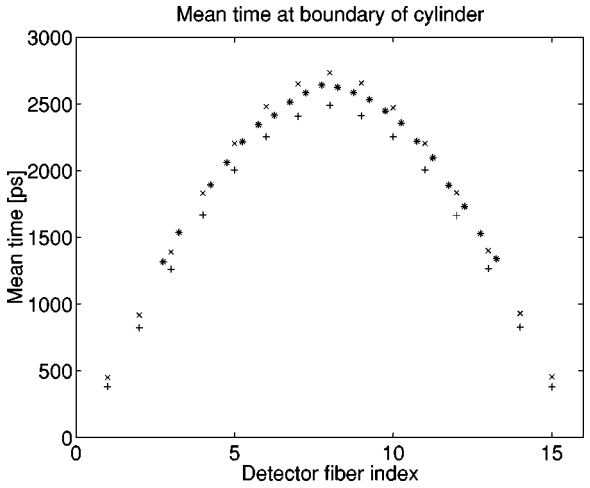

FIG. 8. Comparison between the phase and the mean time measured by MONSTIR. "×" = 760 nm (FD), "+" = 800 nm (FD), "∗" = 780 nm (TD, MONSTIR).

MHz they are reasonably close so that a comparison can be made by calculating the corresponding mean times from the phase using

$$<t> \approx \frac{\varphi}{f_{\mathrm{mod}} \times 360^{\circ}}.$$

In Fig. 8, the mean time data recorded at 780 nm with MONSTIR is illustrated along with the data recorded at 760 and 800 nm with the frequency-domain (FD) system. The differences are mainly due to the different wavelengths used.

VI. DISCUSSION

A frequency-domain measurement system was constructed for medical optical imaging. We introduced a method for avoiding phase-amplitude cross talk by operating the PMT at anode currents lower than 0.1 μA. The current level is set by adjusting the gain of the detector. The lower end of the dynamic range has been increased by minimizing the rf coupling between the source and detector. At 100 MHz, a very low NEP value of 3 fW (0.3 s t.c., 808 nm) was achieved. The practical dynamic range of the system at 100 MHz is $>1{:}10^6$, and both amplitude and phase values are very accurate in this range. The main contributors to the low phase noise are the relatively high quantum efficiency of the H6780-20 detector and close synchronization of the cross-correlation frequency with the clock of the digital lock-in amplifier.

The accuracy of the phase and amplitude were compared with a finite-element solver for the diffusion equation, and the phase values were compared with mean times from a time-resolved tomography system. The residual error of 1.7% may be reduced by improving the finite-element mesh near the boundary and by improving the source model used, perhaps by using a solution of the radiative transfer equation in a small area around each source.[30]

The improved signal-to-noise ratio can be used to shorten measurement time, reduce the light intensity, or improve data quality. A good match between measurements and a forward model is a prerequirement if the optical properties of tissue are to be determined without a reference phantom. Mismatches between the model and the data cause artifacts in the reconstructed images.

Although the instrument itself can measure amplitude to a high accuracy, it is not possible to obtain reliable absolute measurements of amplitude with direct contact of tissue and the optical fibers. Thus, the absolute quantification of scattering and absorption should rely on the phase data. Absolute phase measured at two wavelengths may be sufficient to an approximate solution of the scattering and absorption distributions, since the scattering coefficient varies only a little between two wavelengths in the near infrared. It may be possible to determine the distribution of blood volume and oxygen saturation within a tissue volume based on these measurements.[31] A potential application for the frequency-domain system is the combination of bedside monitoring of cerebral blood volume, oxygen saturation, and the study of the responses of the infant's brain to auditory, somatosensory, or visual stimuli.

ACKNOWLEDGMENTS

The authors would like to thank Tekes, the Academy of Finland, the graduate school Functional Studies in Medicine, and TES for their financial support. The authors are grateful to Dr. Jeremy Hebden for lending out the phantom and data, to Dr. Martin Schweiger and Professor Simon Arridge for the TOAST software, to Professor Matti Kaivola for the many discussions with one of the authors (I.N.) and to Hannu Nissilä for the numerous lessons in mechanical engineering.

[1] F. F. Jöbsis, Science **198**, 1264 (1977).
[2] A. Villringer and B. Chance, Trends Neurosci. **20**, 435 (1997).
[3] S. R. Arridge, Inverse Probl. **15**, R41 (1999).
[4] B. W. Pogue, S. Geimer, T. O. McBride, S. Jiang, U. L. Österberg, and K. D. Paulsen, Appl. Opt. **40**, 588 (2001).
[5] M. Cope, Ph.D. thesis, University College London (1991).
[6] C. H. Schmitz, M. Löcker, J. M. Lasker, A. H. Hielscher, and R. L. Barbour, Rev. Sci. Instrum. **73**, 429 (2002).
[7] A. M. Siegel, J. J. A. Marota, and D. A. Boas, Opt. Express **4**, 287 (1999).
[8] V. Ntziachristos, X. Ma, and B. Chance, Rev. Sci. Instrum. **69**, 4221 (1998).
[9] V. Ntziachristos, X. H. Ma, A. G. Yodh, and B. Chance, Rev. Sci. Instrum. **70**, 193 (1999).
[10] D. Grosenick, H. Wabnitz, H. H. Rinneberg, K. T. Moesta, and P. M. Schlag, Appl. Opt. **38**, 2927 (1999).
[11] H. Eda, I. Oda, Y. Ito, Y. Wada, Y. Oikawa, Y. Tsunazawa, M. Takada, Y. Tsuchiya, Y. Yamashita, M. Oda, A. Sassaroli, Y. Yamada, and M. Tamura, Rev. Sci. Instrum. **70**, 3595 (1999).
[12] F. E. W. Schmidt, M. E. Fry, E. M. C. Hillman, J. C. Hebden, and D. T. Delpy, Rev. Sci. Instrum. **71**, 256 (2000).
[13] T. O. McBride, B. W. Pogue, S. Jiang, U. L. Österberg, and K. D. Paulsen, Rev. Sci. Instrum. **72**, 1817 (2001).
[14] B. Chance, M. Cope, E. Gratton, N. Ramanujam, and B. Tromberg, Rev. Sci. Instrum. **69**, 3457 (1998).
[15] N. Ramanujam, C. Du, H. Y. Ma, and B. Chance, Rev. Sci. Instrum. **69**, 3042 (1998).
[16] Y. Yang, H. Liu, X. Li, and B. Chance, Opt. Eng. (Bellingham) **36**, 1562 (1997).
[17] S. Fantini, M.-A. Franceschini-Fantini, J. S. Maier, S. A. Walker, B. Barbieri, and E. Gratton, Opt. Eng. (Bellingham) **34**, 32 (1995).
[18] E. M. C. Hillman, J. C. Hebden, F. E. W. Schmidt, S. R. Arridge, M. Schweiger, H. Deghani, and D. T. Delpy, Rev. Sci. Instrum. **71**, 3415 (2000).
[19] E. M. C. Hillman, H. Deghani, J. C. Hebden, S. R. Arridge, M. Schweiger, and D. T. Delpy, Proc. SPIE **4250**, 327 (2001).
[20] B. Chance, E. Anday, S. Nioka, S. Zhou, L. Hong, K. Worden, C. Li, T.

Murray, Y. Ovetsky, D. Pidikiti, and R. Thomas, Opt. Express **10**, 411 (1998).
[21] S. R. Hintz, D. A. Benaron, A. M. Siegel, A. Zourabian, D. K. Stevenson, and D. A. Boas, J. Perinat. Med. **29**, 335 (2001).
[22] J. C. Hebden, H. Veenstra, H. Deghani, E. M. C. Hillman, M. Schweiger, S. R. Arridge, and D. T. Delpy, Appl. Opt. **40**, 3278 (2001).
[23] B. W. Pogue, M. Testorf, T. McBride, U. Osterberg, and K. Paulsen, Opt. Express **1**, 391 (1997).
[24] Hamamatsu Photonics, metal package photomultiplier tubes: R7400U series and subminiature photosensor modules (1998).
[25] X. Zhu, E. Krochmann, and J. Chen, Rev. Sci. Instrum. **63**, 1999 (1992).
[26] K. Alford and Y. Wickramasinghe, Rev. Sci. Instrum. **71**, 2191 (2000).
[27] F. E. W. Schmidt, J. C. Hebden, E. M. C. Hillman, M. E. Fry, M. Schweiger, H. Deghani, D. T. Delpy, and S. R. Arridge, Appl. Opt. **39**, 3380 (2000).
[28] J. C. Hebden, M. Tsiraki, and D. T. Delpy, Appl. Opt. **36**, 3802 (1997).
[29] M. Schweiger and S. R. Arridge, Med. Phys. **24**, 895 (1997).
[30] J. P. Kaipio, T. Vilhunen, M. Vauhkonen, and V. Kolehmainen, *OSA Biomedical Topical Meeting Technical Digest* (Optical Society of America, Washington, DC, 2002), pp. 12–14.
[31] E. M. C. Hillman, S. R. Arridge, J. C. Hebden, and D. T. Delpy, *OSA Biomedical Topical Meeting Technical Digest* (Optical Society of America, Washington, DC, 2002), pp. 599–601.